THE JOURNAL OF BIOLOGICAL CHEMISTRY VOL. 283, NO. 51, pp. 36046–36059, December 19, 2008

Multiple Kv Channel-interacting Proteins Contain an N-terminal Transmembrane Domain That Regulates Kv4 Channel Trafficking and Gating*

Received for publication, September 4, 2008, and in revised form, October 22, 2008 Published, JBC Papers in Press, October 28, 2008, DOI 10.1074/jbc.M806852200

Henry H. Jerng[1] **and Paul J. Pfaffinger**

From the Department of Neuroscience, Baylor College of Medicine, Houston, Texas 77030

Kv channel-interacting proteins (KChIPs) are auxiliary subunits of the heteromultimeric channel complexes that underlie neuronal I_{SA}, the subthreshold transient K^+ current that dynamically regulates membrane excitability, action potential firing properties, and long term potentiation. KChIPs form cytoplasmic associations with the principal pore-forming Kv4 subunits and typically mediate enhanced surface expression and accelerated recovery from depolarization-induced inactivation. An exception is KChIP4a, which dramatically suppresses Kv4 inactivation while promoting neither surface expression nor recovery. These unusual properties are attributed to the effects of a K channel inactivation suppressor domain (KISD) encoded within the variable N terminus of KChIP4a. Here, we have functionally and biochemically characterized two brain KChIP isoforms, KChIP2x and KChIP3x (also known as KChIP3b) and show that they also contain a functional KISD. Like KChIP4a and in contrast with non-KISD-containing KChIPs, both KChIP2x and KChIP3x strongly suppress inactivation and slow activation and inhibit the typical increases in surface expression of Kv4.2 channels. We then examined the properties of the KISD to determine potential mechanisms for its action. Subcellular fractionation shows that KChIP4a, KChIP2x, and KChIP3x are highly associated with the membrane fraction. Fluorescent confocal imaging of enhanced green fluorescent proteins (eGFP) N-terminally fused with KISD in HEK293T cells indicates that KISDs of KChIP4a, KChIP2x, and KChIP3x all autonomously target eGFP to intracellular membranes. Cell surface biotinylation experiments on KChIP4a indicate that the N terminus is exposed extracellularly, consistent with a transmembrane KISD. In summary, KChIP4a, KChIP2x, and KChIP3x comprise a novel class of KChIP isoforms characterized by an unusual transmembrane domain at their N termini that modulates Kv4 channel gating and trafficking.

The subthreshold A-type current (I_{SA})[2] in neurons regulates membrane excitability, modulates action potential spike frequency, and participates in dendritic signal integration (1). The I_{SA} channel is formed from Kv4 pore-forming α-subunits partnered with modulatory subunits, most critically the dipeptidyl peptidase-like proteins (DPLPs) and Kv channel-interacting proteins (KChIPs) (2–4). In general, isoforms of both DPLPs and KChIPs promote trafficking of Kv4 subunits to the plasma membrane and greatly enhance Kv4 current expression. However, both DPLPs and KChIPs exist as splice variants with alternative N-terminal domains that can exert profound differential effects on channel functional properties (1, 5–8).

All KChIPs contain an invariant KChIP core domain that functions, as shown by recent x-ray crystallography results, by binding and sequestering the Kv4 N terminus and stabilizing the Kv4 tetramer by laterally clamping adjacent tetramerization (T1) domains (9–12). The Kv4 N terminus acts both as an ER retention signal (13) as well as an endogenous inactivation particle (14). KChIP binding overrides the activities of the Kv4 N terminus and leads to increases in surface expression and remodeling of inactivation kinetics (15).

An extraordinary KChIP4 variant known as KChIP4a has been reported to interact with Kv4 α-subunits and mediate an exceptionally slow inactivation previously unseen with other KChIPs, including other KChIP4 variants (7). This effect of KChIP4a has been attributed to novel functional effects of the K channel inactivation suppressor (KIS) domain that is encoded in the 34-amino acid alternative N terminus of this KChIP4 variant. Kinetic analysis results show that KChIP4a also slows channel opening, disrupts rapid inactivation of opened channels, and interferes with channel closing. KChIP4a probably affects I_{SA} kinetics in native neurons in a similar manner, since the expression of KChIP4a transcripts in neurons from globus pallidus and basal forebrain is associated with a slowly inactivating I_{SA} component and slower I_{SA} deactivation kinetics (16). Indeed, heterologous expression studies suggest that in native neurons differential expression of DPLP and KChIP splice variants could regulate inactivation kinetics over a range of 100-fold (7, 8). In addition to the kinetic effects, KChIP4a-bound Kv4 channels tend to traffic poorly to the cell surface and

* This work was supported, in whole or in part, by National Institutes of Health Grant PO1 NS37444. Some of the data presented here have previously appeared in abstract form (17). The costs of publication of this article were defrayed in part by the payment of page charges. This article must therefore be hereby marked "*advertisement*" in accordance with 18 U.S.C. Section 1734 solely to indicate this fact.

[1] To whom correspondence should be addressed: Dept. of Neuroscience, Baylor College of Medicine, One Baylor Plaza, S630, Houston, TX 77030. Tel.: 713-798-3062; Fax: 713-798-3946; E-mail: hjerng@cns.bcm.tmc.edu.

[2] The abbreviations used are: I_{SA}, subthreshold A-type current; KChIP, Kv channel-interacting protein; DPLP, dipeptidyl peptidase-like proteins; KIS, K channel inactivation suppressor; KISD, K channel inactivation suppressor domain; tmKChIP, type I transmembrane KChIP; GFP, green fluorescent protein; eGFP, enhanced green fluorescent protein; CMV, cytomegalovirus; ER, endoplasmic reticulum.

instead prefer to remain in the endoplasmic reticulum or the Golgi apparatus (13). What additional role this regulation of trafficking plays in native neurons is not clear.

Here we identify two additional KChIP isoforms (KChIP2x and KChIP3x) with high N-terminal sequence homology to the KChIP4a KISD. By coexpression studies, we determined that, like KChIP4a, KChIP2x, and KChIP3x, both possess a functional KISD capable of dramatically slowing down inactivation kinetics and interfere with the core-dependent promotion of surface expression. We then examined the biochemical properties of the KISD and show that the KISD is a transmembrane domain that completely spans the lipid bilayer and is capable of targeting soluble eGFP to membranes. In summary, our results highly suggest that the unusual kinetic and trafficking properties associated with the KISD depend on its transmembrane nature.

EXPERIMENTAL PROCEDURES

Molecular Biology—The following cDNAs were acquired or generated for functional studies in *Xenopus* oocytes. Rat Kv4.2 cDNA in pBluescript SK was obtained as previously described (4). Human KChIP3a and KChIP4b-L cDNAs were purchased from the American Type Culture Collection (Manassas, VA) and maintained in pT7T3D-Pac and pBSR, respectively. Human KChIP4a cDNA was generated by replacing exon 1 of 4b-L for that of 4a (KISD). KChIP2x and KChIP3x (KChIP3b) cDNAs were PCR-amplified from whole brain cDNA libraries generated from p21 Sprague-Dawley rats. PCR forward and reverse primers always contained nested restriction enzyme sites to allow the KChIP2x and KChIP3x cDNAs to be subcloned into pT7T3D-Pac.

For mammalian cell expression in HEK293T cells, various cDNAs were subcloned into plasmid vectors with protein translation driven by the CMV promoter. pEGFP-N1 (pCMV-EGFP-N1) was purchased from Clontech, and human KChIP3a cDNA was subcloned into pCMV-EGFP-N/C (Clontech), replacing the eGFP open reading frame. Human KChIP4a and rat KChIP2x and KChIP3x cDNAs were PCR-amplified from the cDNA library previously described with the appropriate nested restriction enzyme sites for subcloning into pCMV-EGFP-N/C. Rat DPP6a (DPPX-E) and DPP6-S (DPPX-S) cDNAs were amplified by PCR from cDNA library and subcloned into pCMV-EGFP-N/C vector. Exon 1 of KChIP4a (4aNt), KChIP3x (3xNt), KChIP2x (2xNt), and KChIP4e (4eNt) were PCR-amplified and subcloned into pCMV-EGFP-N1 in frame with the eGFP open reading frame to create exon 1-eGFP fusion proteins. For surface biotinylation, cysteine substitutions in KChIP4a N terminus, including KChIP4a/N2C, KChIP4a/E4C, and KChIP4a/N2C/E4C, were generated using the QuikChange site-directed mutagenesis kit (Stratagene, La Jolla, CA). All DNA constructs were sequence-verified by automated sequencing (sequencing core facility of Baylor College of Medicine) and confirmed to be correct.

Data Base Mining and Sequence Analysis—Data base mining for KChIP isoforms with N-terminal sequence similar to that of KChIP4a KISD yielded a KChIP2 isoform encoded by a human expressed sequence tag cDNA from adult nervous tumor (accession number BF919228). The same novel KChIP2 isoform was also described by a chimpanzee mRNA (accession number XM_001170567). This isoform was named KChIP2x. The same strategy yielded KChIP3x, an isoform previously named as KChIP3b (5). KChIP3x was identified as expressed sequence tag clones from human, mouse, rat, and cow (accession numbers CB615550, CJ058519, BB658948, DT821924, and AL540923). Interestingly, the organ sources for the expressed sequence tag clones are diverse and outside of the central nervous system, including dorsal root ganglia, heart, ileum, and placenta, agreeing with the reverse transcription-PCR results of Pruunsild and Timmusk (5) that showed that KChIP3x is expressed outside as well as inside the brains of humans (*i.e.* colon, heart, kidney, placenta, prostate, salivary gland, stomach, testis, and thymus) and mice (*i.e.* heart, kidney, lung, testis, and thymus).

The MEMSAT3 program was used to predict transmembrane topology, available at The PSIPRED Protein Structure Prediction Server (available on the World Wide Web)

Electrophysiology—Run-off cRNA transcripts were synthesized from linearized plasmid DNAs using the mMessage mMachine high yield capped RNA transcription kit (Ambion, Austin, TX). T7 or T3 RNA polymerase was used, depending on the plasmid. Kv4.2 cDNA, with or without an equimolar amount of KChIP cRNAs, was injected into stage V and VI defolliculated *Xenopus* oocytes using a Nanoinjector (Drummond, Broomall, PA). Afterward, injected oocytes were maintained at 18 °C for 1–2 days in standard ND 96 solution (96 mM NaCl, 2 mM KCl, 1.8 mM $CaCl_2$, 1 mM $MgCl_2$, and 5 mM HEPES, pH 7.4, adjusted with NaOH) supplemented with 5 mM sodium pyruvate and 5 μg/ml gentamycin.

A two-electrode voltage clamp technique was implemented to elicit whole-cell currents from injected oocytes. Bathed in normal ND96 solution, the oocytes were impaled by microelectrodes (<1 megaohm resistance) filled with 3 M KCl solutions, and studied at room temperature (22–23 °C). Voltage clamp protocols were controlled by either pClamp6 (Axon Instruments, Union City, CA) or WinWCP (John Dempster, University of Strathclyde, Glasgow, UK) and delivered by oocyte clamp OC-725 (Warner Instruments, Hamden, CT). The analog data were digitized and low pass-filtered before acquisition (Frequency Devices, Haverhill, MA). Average leak current was <0.2 μA, and the capacitance transients and leak currents were subtracted off-line using appropriately scaled up traces at voltages without ionic currents (at −90 mV).

Transfections and Western Blotting—Human embryonic kidney (HEK293T) cells were cultured in DMEM+GlutaMAX™-1 (Dulbecco's modified Eagle's medium plus 4.5 g/liter D-glucose and 110 mg/liter sodium pyruvate; catalog number 10569; Invitrogen) supplemented with 10% fetal bovine serum (Invitrogen), 100 units/ml penicillin, and 100 units/ml streptomycin at 37 °C in humidified 5% CO_2 atmosphere. HEK293T cells were transfected using Lipofectamine 2000 reagent (Invitrogen), following precisely the manufacturer's protocols. Heterologous expression of proteins was tested 48 h after transfection by Western blot analysis, following a previously described protocol (4). Primary anti-pan-KChIP (K55/82; Antibodies Inc., Davis, CA), anti-eGFP (3E6; Invitrogen), anti-KChIP3 (FL-214; Santa Cruz Biotechnology, Inc., Santa Cruz,

CA), and anti-DPP6 antibodies (ab41811; Abcam; Cambridge, MA) were used at 1:1000 dilutions. After treatment with appropriate secondary horseradish peroxidase-conjugated antibodies, the bound antibodies were detected by chemiluminescence with an ECL detection kit (SuperSignal West Pico Chemiluminescent Substrate; Thermo Fisher Scientific).

Fluorescent Confocal Microscopy—Twenty-four hours post-transfection, HEK293T cells were trypsinized and reseeded on 24-well clusters with poly-L-lysine-coated glass coverslips and allowed to attach for 24–36 h. Cells were viewed under fluorescence on an Olympus BX51WI upright microscope with a ×60 water immersion objective, and images were captured using the FluoView FV300 confocal imaging software package on a desktop PC.

Crude Membrane Preparation—Two days post-transfection, the cells were washed two times with precooled phosphate-buffered saline solution containing calcium and magnesium (PBS/CM; 137 mM NaCl, 2.7 mM KCl, 8 mM Na_2HPO_4, 1.5 mM KH_2PO_4, 0.1 mM $CaCl_2$, 1 mM $MgCl_2$, pH 7.0, with HCl). The cells were then scraped into 1.2 ml of ice-cold homogenization buffer (10 mM Tris-HCl, 1 mM EDTA, pH 7.4) plus protease inhibitors (Complete protease inhibitor mixture tablet; Roche Applied Science). Afterward, the cells were homogenized by hand using a Dounce homogenizer for 12–15 strokes or until a homogenous suspension is achieved, followed by centrifugation at 500 × *g* for 5 min at 4 °C to remove nuclei, cell debris, and unbroken cells. The supernatant was then centrifuged at 45,000 × *g* for 30 min at 4 °C to pellet the membranes, and the resulting pellet was resuspended in 100 μl of homogenization buffer. The protein concentrations were estimated using the BCA assay (MicroBCA™ assay kit; Thermo Fisher Scientific), and aliquots were stored at −80 °C.

Cell Surface Biotinylation—All solutions used throughout the procedure were kept ice-cold. After 48 h of incubation, transfected cells were washed two times with 2 ml of PBS/CM. For permeabilized cells, cells were first incubated in 1 ml of PBS/CM with 0.1% Triton X-100 for 1 min followed by incubation in, 2 ml of PBS/CM with fresh 6 mM Tris (2-carboxyethyl)-phosphine (pH 7.0) for 12 min at 4 °C. The TCEP solution was removed, and the cells were incubated in 1 ml of fresh 1 mg/ml maleimide-PEO2-biotin (Pierce) diluted in PBS/CM for 1 h. To ensure complete quenching of unreacted reagent, the cells were treated with 1 ml of PBS/CM with fresh 5 mM dithiothreitol for 20 min. Afterward, the cells were washed twice with ice-cold PBS/CM before being recovered by centrifugation at 166 × *g* for 5 min at 4 °C.

The recovered HEK293T cells were lysed in 400 ml of lysis buffer at 4 °C for 1 h (Lysis buffer: 150 mM NaCl, 50 mM Tris-HCl, 1% Triton X-100, 0.1% SDS, and protease inhibitor). To remove insoluble material, the lysates were centrifuged at 15,800 × *g* for 30 min at 4 °C. The lysate are then collected, and 20-μl aliquots were saved for gel analysis. Equilibrated streptavidin-agarose beads (50 μl; Novagen) were added to the lysate, and the mixture was incubated overnight at 4 °C with constant mixing. The following day, the beads were extensively washed with lysis buffer by centrifugation at 500 × *g* for 5 min. After three or four washes, 50 ml of 2× Laemmli sample buffer was added (sample buffer, 2×: 100 mM Tris-HCl, pH 6.8; 20% (v/v) glycerol; 4% (w/v) SDS; 200 mM dithiothreitol, and 0.2% (w/v) bromphenol blue, pH 6.8). The bound proteins were eluted from the beads by boiling at 100 °C for 5 min. The eluted proteins were separated on SDS-PAGE and prepared for Western blotting as described previously.

Molecular Modeling—Kv4.2 plus KChIP structural model was constructed by combining the KChIP1-Kv4.3 T1 structural model (12) with the Kv1.2 structural model (21). Initially, the transmembrane domain of Kv4.2 was threaded onto the S1–S6 region of the Kv1.2 model using the DeepView (22) server, which also provided potential loop structures for missing segments. This model was then made tetrameric, and side chain clashes were removed using the NAnoscale Molecular Dynamics simulation package (23) (available on the World Wide Web). The Kv4.2 T1 and KChIP2 sequences were then threaded on the KChIP1-Kv4.3 T1 structure using DeepView, which also provided potential missing loop structures. Next, the T1 domain of the KChIP2-Kv4.2 T1 model was fit to the Kv1.2 T1 domain model by root mean square deviation minimization, and this transform was used to move the KChIP4-Kv4.2 T1 model into registration below the channel. We then combined the transmembrane and T1 domain models for Kv4.2 by insertion of a linker segment between T1 and S1. Because of the presence of a Zn^{2+} site in the Kv4.2 T1 domain, forming a connection between channel and T1 domain with the length of chain available required a registration between the T1 domain and the TM domain of the same subunit different from what is seen in the Kv1.2 model. In the Kv1.2 model, these two domains are 90° rotated, whereas in the Kv4.2 model, they are on top of each other. The completed model was solvated, inserted into a POPC bilayer, and ionized with 150 mM KCl using VMD/NAnoscale Molecular Dynamics (23). The model was then minimized and equilibrated using NAnoscale Molecular Dynamics run on the Lonestar server (TACC through Teragrid). To model the KISD, an α-helical model was constructed inserted into a lipid bilayer model identical to that used for the channel and then minimized and equilibrated. These models were combined by docking the KIS model onto the side of the Kv4.2 transmembrane model and constructing a loop between the KISD and the KChIP core using the remaining sequence of KChIP4a. The combined solvated, membrane-inserted, and ionized structure was minimized, equilibrated, and simulated for over 4 ns. Model figures were made using VMD and Pov-Ray (Persistence of Vision Pty., Ltd.).

Data Analyses—Peak conductance (G_p) was calculated as $G_p = I_p/(V_c - V_{rev})$, where I_p is the peak current, V_c is the command voltage, and V_{rev} is the reversal potential (−90 mV in ND96). Peak conductance-voltage (*G*-V) curves were described using the first-order Boltzmann function: $G_p/G_{p(max)} = 1/(1 + \exp(V_m - V_a)/k))$, where G_p/G_{max} is the fraction of maximal conductance, V_m is the membrane potential, V_a is the potential for half-maximal activation, and k is the slope factor. Steady-state inactivation was measured with 10-s-long conditioning pulses at the indicated potentials before pulsing to +50 mV to determine the amount of current inactivation. Steady-state inactivation is described using a single Boltzmann function, generating potential for half-maximal inactivation (V_i) and slope (k). The time courses of recovery from inactivation were

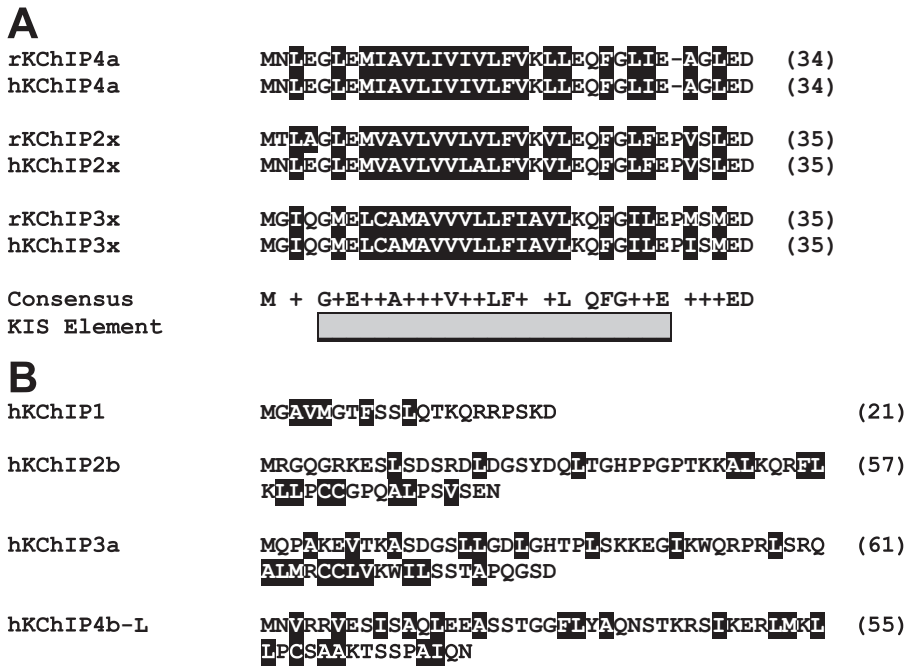

FIGURE 1. **KChIP2x and KChIP3x share strong sequence similarities with KChIP4a at their variable N-terminal domains.** Hydrophobic residues are indicated with black background, and *numbers* in *parentheses* represent the position of the final residue shown. *A*, exon 1 sequence alignment of KChIP4a, KChIP2x, and KChIP3x from rats (*r*) and humans (*h*). Exon 1 of KChIP4a encodes the complete KISD. Identical residues are indicated in the consensus sequence, and sequence conservation is shown as *plus signs*. *B*, typical KChIP isoforms (KChIP1, KChIP2b, KChIP3a, and KChIP4b-L) have no extended stretch of hydrophobic residues.

measured using a two-pulse protocol. Briefly, two pulses to +50 mV (inactivating pulse and test pulse) were separated by a variable recovery interval at −100 mV to determine the time required for channel recovery. The results for recovery from inactivation were fitted with single exponential functions. Time courses of activation and inactivation were respectively measured by time points where half of the current activated ($t_{0.5a}$) or inactivated ($t_{0.5i}$). In addition, activation kinetics were also described by exponential fitting of the 50–90% of the current rising phase, yielding τ (50–90%). Data are presented as means ± S.E. The number of experiments analyzed (*n*) is indicated in Table 1.

RESULTS

Identification of Additional KChIPs with KISD-like Motifs—The most pronounced and distinguishing features of KChIP4a-modified Kv4 current are an exceptionally slow kinetics of inactivation at depolarized potentials along with an absence of accelerated recovery commonly associated with KChIP modulation (7). These KChIP effects are attributed to a hypothesized KISD contained in the 34 amino acids of the variant N terminus of the KChIP4a isoform. In addition to gating effects, KChIP4a also suppresses the enhanced surface expression of channels normally seen with other KChIP variants, again presumably due to the action of the KISD (7, 13). In the process of performing evolutionary conservation analysis on this domain, we have identified additional N-terminal KChIP variants with significant sequence similarity to the KChIP4a KISD. Both the genes of KChIP2 and KChIP3, but not of KChIP1, were found to express N-terminal variants homologous to KChIP4a (Fig. 1*A*). Since other variants in these genes already have the "a" designation, we have named these new variants KChIP2x and KChIP3x.

The alignment of exon 1 amino acid sequences from the rat and human versions of KChIP4a, KChIP2x, and KChIP3x reveals a striking degree of sequence conservation. (Fig. 1*A*). More than one-third of the residue positions are identical among the N-terminal domains of KChIP4a, KChIP2x, and KChIP3x (shown in canonical sequence and according to KChIP4a numbering: Gly^5, Glu^7, Ala^{10}, Val^{14}, Leu^{17}, Phe^{18}, Leu^{22}, Gln^{24}, Phe^{25}, Gly^{26}, Glu^{29}, Glu^{33}, and Asp^{34}). Two canonical residues (Gly^5 and Glu^{29} of KChIP4a) flank a 25-amino acid-long stretch of highly conserved (>90%) and mostly hydrophobic residues (Fig. 1*A*). This conserved hydrophobic segment, which we call the KIS element, appears to be a defining feature responsible for suppression of Kv4 inactivation and other KISD-mediating functional effects. It is important to note that the high degree of conservation between the N-terminal domains of KChIP4a, KChIP2x, and KChIP3x is in marked contrast when compared with those of other KChIP isoforms that share little to no sequence conservation at their N termini and are composed of mostly polar or charged hydrophilic residues (Fig. 1*B*).

The sequence alignment also reveals discrete differences between the potential KIS elements of KChIP4a, KChIP2x, and KChIP3x. First, a proline residue (Pro^{30}) is present in KChIP2x and KChIP3x immediately following the C terminus-flanking Glu^{29} but not KChIP4a (Figs. 1*A*). Conserved proline residues often produce important structural kinks into proteins; therefore, Pro^{30} may result in KChIP2x and KChIP3x sharing certain common effects on Kv4 channels that are not seen with KChIP4a or KChIP4e. Second, Lys^{20} of KChIP4a is conserved in KChIP2x but is nonconservatively substituted to an Ala in KChIP3x, potentially providing the KChIP3x KISD with novel functional properties.

Functional Effects of KIS Element-containing KChIPs on Kv4.2 Channel Kinetics—To test whether the potential KIS elements located in KChIP2x and KChIP3x also function as KISDs, we co-expressed Kv4.2 α-subunits with various KChIP auxiliary subunits and measured whole oocyte current under voltage clamp conditions. *Xenopus* oocytes were injected with Kv4.2 cRNAs alone or with KChIP cRNAs indicated in Fig. 2 in a 1:1 cRNA molar ratio. Oocytes injected with Kv4.2 cRNA alone expressed depolarization-activated currents that rise and decay rapidly to a non-zero steady-state level (Fig. 1*C*). With step depolarizations, Kv4.2 current becomes evident at approximately −60 mV, and increasing depolarization is accompanied

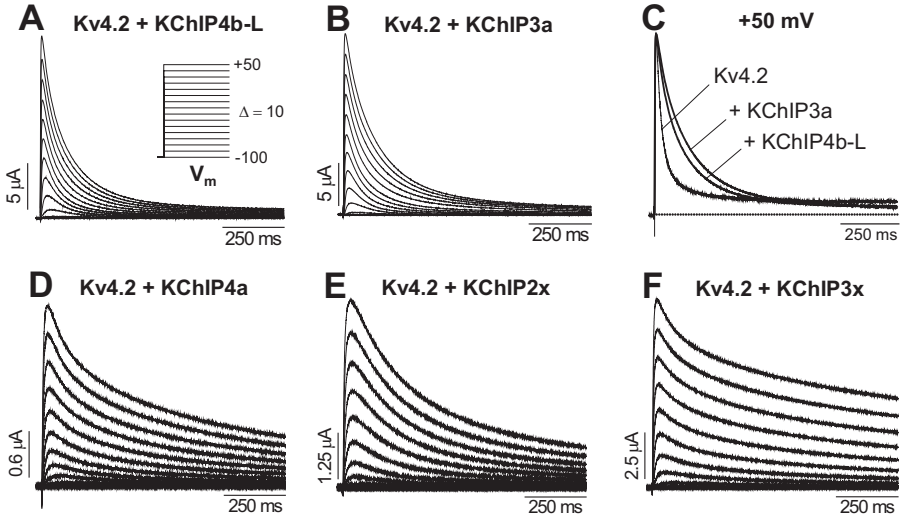

FIGURE 2. **As in KChIP4a, the N-terminal domains of KChIP2x and KChIP3x contain functional KISDs.** *A*, outward currents from oocytes coexpressing Kv4.2 and KChIP4b-L, a representative typical KChIP, elicited by depolarizing voltage pulses indicated in the *inset*. The full duration was 1 s. *B*, current mediated by Kv4.2 + KChIP3a channels observed with the same pulse protocol as in *A*. *C*, normalized and overlapped traces at +50 mV for Kv4.2 alone, Kv4.2 + KChIP4bL, and Kv4.2 + KChIP3a, showing similar inactivation slowing by these non-KISD-containing variants. *D–F*, representative current traces of Kv4.2 + KChIPa, Kv4.2 + KChIP2x, and Kv4.2 + KChIP3x channels, respectively. Like KChIP4a, KChIP2x and KChIP3x dramatically slow Kv4.2 inactivation more than the typical KChIPs.

by accelerated kinetics of both activation and inactivation, resulting in the typical Kv4 A-type current.

To identify unique functional effects of encoded KISDs, we compared the functional effects of our putative KISD-containing KChIPs with non-KISD-containing subunits, KChIP4b-L (long) and KChIP3a, beginning with inactivation kinetics. In general, non-KISD-containing KChIPs moderately slow the kinetics of Kv4.2 inactivation by disengaging the endogenous N-type-like inactivation mechanism through an entrapment of the N-terminal inactivation particle by the KChIP core domain (1), but the kinetics of the remaining non-N-type inactivation vary moderately, depending on the KChIP core domain (2). In agreement, Kv4.2 channels expressed with KChIP3a inactivate more slowly than those expressed with KChIP4b-L (Fig. 2, *A–C*). To compare the inactivation kinetics, we used the time when half of the peak current is inactivated (half-inactivation time) since inactivation kinetics of Kv4.2 channels in the presence of various KChIP subunits in this study cannot be adequately fit with the same number of exponential functions. The half-inactivation times for non-KISD-containing KChIPs range from around 50 to 100 ms (at +40 mV: Kv4.2 + KChIP4b-L, 87 + 4.5 ms (n = 5); Kv4.2 + KChIP3a, 104 + 2.4 ms (n = 8); and published values for *Xenopus* expression of Kv4.2 + KChIP1, 54 + 5.6 ms, and Kv4.2 + KChIP2, ~47.9 ms (from single exponential fits) (3, 24). These results indicate that among non-KISD-containing KChIP variants, KChIP3a and KChIP4b-L mediates slower inactivation kinetics, and the functional effects of the N-terminal KISD can be appreciated by comparison with either of these variants. Fig. 2*D* shows that, as reported previously (7, 8), KChIP4a dramatically slows the inactivation kinetics of Kv4.2 currents to an extent that inactivation remains incomplete even after a 1-s-long depolarization. At more depolarized potentials (0 mV and above), the inactivation decay kinetics are clearly double exponential. In contrast, the KChIP4b-L and KChIP3a N-terminal variants mediate significantly less inactivation slowing than KChIP4a, with inactivation essentially monoexponential and complete within 1 s (Fig. 2, compare *D* with *A* and *B*).

We next examined the functional effects of the new KIS element-containing KChIPs. As Fig. 2*E* shows, co-expression of KChIP2x and Kv4.2 results in a slowly activating and slowly inactivating Kv4.2 current. Similar to KChIP4a, inactivation mediated by KChIP2x is incomplete within 1 s, but unlike KChIP4a the decay is less clearly biexponential. Meanwhile, co-expression of Kv4.2 of KChIP3x results in an even more dramatic disruption of the inactivation process (Fig. 2*F*). At the end of a 1-s depolarization to +50 mV, more than half of the current remains, compared with the complete inactivation seen following co-expression of Kv4.2 with the non-KISD-containing variant KChIP3a (Fig. 2, compare *F* and *B*; Fig. 3*A*). Altogether, these results suggest that the putative KIS sequence present in these subunits appears to act as functional KISDs.

Differential Effects of KISDs on the Kinetics and Voltage Dependence of Channel Gating—Fig. 3 summarizes the quantitative differences between functional effects of the different KISD-containing variant subunits. For purposes of this figure, we designated KChIP3a as the representative non-KISD-containing KChIP for biophysical comparisons (for comparisons against KChIP4b-L, see Table 1). KChIP4a, KChIP2x, and KChIP3x all mediate markedly slower inactivation when compared with KChIP3a. As the overlapped normalized traces at +50 mV indicate, KChIP3x mediates the greatest amount of inactivation slowing, followed closely by KChIP2x and KChIP4a. The half-inactivation time for KChIP3x, KChIP2x, and KChIP4a are ~1000 ms, ~450 ms, and ~400 ms, respectively, 4–10 times slower than KChIP3a (Fig. 3*B* and Table 1). Moreover, the voltage dependence of half-inactivation time reveals an interesting property of KChIP-associated Kv4.2 channels. In the presence of KChIP4a, KChIP2x, KChIP3x, and KChIP3a, Kv4.2 inactivates with an inverse voltage dependence, where increases in voltage result in decreases in inactivation rate. In contrast, Kv4.2 inactivation accelerates with increasing voltage (8, 25). This inverse voltage dependence appears to be characteristic of the Kv4 closed state inactivation mechanism, which becomes increasingly less effective with increasing depolarization (25–27). This result suggests that the primary effect of the KISD is to slow the kinetics of the closed state inactivation pathway, probably via slowed channel closing (7), after the KChIP core sequesters the N-type-like inactivation mechanism.

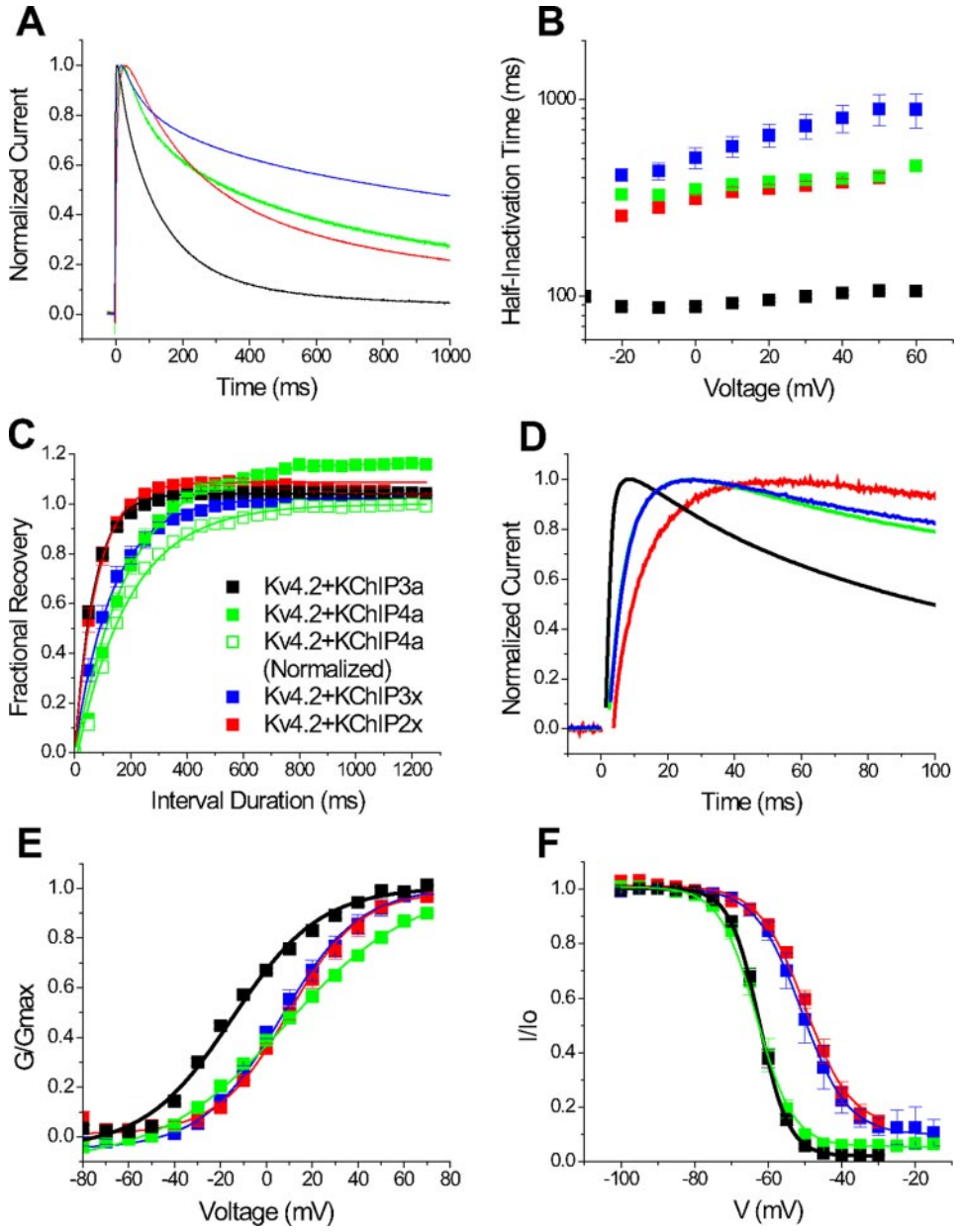

FIGURE 3. **KISDs of KChIP4a, KChIP2x, and KChIP3x exert differential effects on the kinetics and voltage dependence of channel gating.** *Color coding* of current traces and analyzed data are as described in the *key* shown in *C*. Functional properties of KISD-containing KChIPs are compared with the non-KISD-containing KChIP3a. Voltage step protocols are described in detail under "Experimental Procedures." *A*, normalized and superimposed current traces at +50 mV for Kv4.2 coexpressed with the indicated KChIP isoforms. Kv4.2 channels inactivate exceptionally more slowly when coexpressed with KChIP4a, KChIP2x, and KChIP3x. *B*, relationship between membrane voltage and inactivation, measured by the time point when half of the current inactivates (half-inactivation time). *C*, recovery from inactivation at −100 mV as determined by a two-pulse protocol. The *curves* represent results of best single-exponential fits. *D*, kinetics of current rise upon depolarization to +50 mV, after normalization and superimposition. *E*, normalized peak conductance (G/G_{max}) at various voltages. The peak conductance-voltage relationships were described by Boltzmann functions and indicated as *fitted curves*. *F*, voltage dependence of steady-state inactivation. *Curves* are Boltzmann fits.

various KChIP isoforms under study using a two-pulse protocol. In agreement with Holmqvist *et al.* (7), we find that KChIP4a co-expression does not accelerate the recovery from inactivation of Kv4.2 channels (Table 1), suggesting that the KChIP4a KISD prevents the KChIP4 core-mediated acceleration of recovery (Fig. 3*C*). Although Kv4.2 + KChIP4a current exhibited a dramatic "overshoot" of recovery from inactivation (where recovered current amplitude is greater than that of the initial current), after normalization, the recovery kinetics is not statistically different from that of Kv4.2 alone. In contrast to KChIP4a, KChIP2x and KChIP3x do accelerate the time course of recovery from inactivation (Table 1 and Fig. 3*C*). In particular, KChIP2x-mediated recovery from inactivation is just as rapid as that mediated by the non-KISD-containing KChIP3a. This result strongly suggests that the regulation of recovery mediated by the KISD is sequence-specific and separate from its effects on slowing of inactivation. Interestingly, an overshoot is also observed with recovery from inactivation mediated by KChIP2x (Fig. 3*C* and Table 1).

Macroscopic and single-channel data have indicated that the KISD of KChIP4a significantly disrupts the activation of Kv4.3 channels, as indicated by an increased latency to first opening or progressive ramp-like opening (7). Kv4.2 currents modified by KChIP4a, KChIP2x, and KChIP3x all exhibit marked slowing of kinetics of activation when compared with KChIP3a-modified currents (Fig. 4*D*). The slowed activation is associated with increased time to reach the peak current measured at +50 mV. Quantitatively, the KISD of KChIP2x produce more slowing of Kv4.2 activation than KChIP4a or KChIP3x (Table 1).

In addition to differential effects on inactivation time course, the KISD-containing variants also differentially regulate recovery from inactivation. Holmqvist *et al.* (7) reported that KChIP4a does not accelerate recovery from inactivation of Kv4.3 channels, unlike non-KISD KChIPs, suggesting that the KChIP4a KISD antagonizes this normal function of the KChIP core domain. We therefore measured the recovery from inactivation for Kv4.2 channels at −100 mV in the presence of the

The observed differences in modulation of Kv4.2 kinetic properties suggested that KISD-containing variants may also differentially modify the voltage dependence of activation and inactivation. Peak conductance-voltage relationships of Kv4.2 channels co-expressed with the different mutants are plotted as a function of membrane potential (Fig. 4*E*). The data show that

TABLE 1
Differential modulation of Kv4.2 channel properties by KChIP isoforms
See "Data Analyses" for descriptions of the parameters measured. Data are mean ± S.E.

	Kv4.2	Kv4.2 + KChIP4b-L	Kv4.2 + KChIP3a	Kv4.2 + KChIP4a	Kv4.2 + KChIP2x	Kv4.2 + KChIP3x
***G*-V relation**						
V_a (mV)	-3.6 ± 1.3	-17.1 ± 0.7^{a}	-17.4 ± 0.9^{a}	$8.0 \pm 0.6^{a,b}$	$12.3 \pm 2.5^{a,b}$	$6.5 \pm 2.3^{a,b}$
k (mV/*e*-fold)	23.1 ± 1.6 ($n = 6$)	17.9 ± 0.8^{a} ($n = 4$)	20.4 ± 0.8 ($n = 10$)	27.5 ± 0.4^{b} ($n = 4$)	$15.5 \pm 1.0^{a,b}$ ($n = 4$)	17.3 ± 1.4 ($n = 3$)
Prepulse inactivation						
V_i (mV)	-66.3 ± 0.9	$-59.5 \pm 0.9^{a,b}$	-61.5 ± 0.5^{a}	-62.1 ± 0.8^{a}	$-49.3 \pm 1.5^{a,b}$	$-50.3 \pm 1.9^{a,b}$
k (mV/*e*-fold)	4.4 ± 0.1 ($n = 3$)	$3.4 \pm 0.04^{a,b}$ ($n = 4$)	3.6 ± 0.1^{a} ($n = 22$)	$3.9 \pm 0.1^{a,b}$ ($n = 3$)	$6.1 \pm 0.3^{a,b}$ ($n = 3$)	$5.2 \pm 0.2^{a,b}$ ($n = 3$)
Inactivation kinetics at +50 mV						
$t_{0.5i}$ (ms)	26 ± 1.2 ($n = 6$)	$88 \pm 4.7^{a,b}$ ($n = 5$)	107 ± 2.8^{a} ($n = 8$)	$409 \pm 20^{a,b}$ ($n = 7$)	$382 \pm 21^{a,b}$ ($n = 7$)	$879 \pm 162^{a,b}$ ($n = 7$)
Activation kinetics at +50 mV						
$t_{0.5a}$ (ms)	3.9 ± 0.3 ($n = 6$)	$2.5 \pm 0.0^{a,b}$ ($n = 3$)	3.2 ± 0.2 ($n = 8$)	$5.8 \pm 0.2^{a,b}$ ($n = 8$)	$10 \pm 1.0^{a,b}$ ($n = 8$)	$6.0 \pm 0.7^{a,b}$ ($n = 6$)
τ (50–90%) (ms)	1.10 ± 0.04 ($n = 18$)	ND[c]	0.94 ± 0.04^{a} ($n = 13$)	$4.70 \pm 0.25^{a,b}$ ($n = 7$)	$10.9 \pm 0.64^{a,b}$ ($n = 5$)	$3.94 \pm 0.59^{a,b}$ ($n = 7$)
Recovery from inactivation at −100 mV						
τ (ms)	221 ± 5 ($n = 3$)	$52 \pm 7^{a,b}$ ($n = 5$)	77 ± 1^{a} ($n = 9$)	194 ± 13^{b} ($n = 8$)	70 ± 7^{a} ($n = 3$)	$125 \pm 18^{a,b}$ ($n = 3$)
Overshoot (%)	3.3 ± 0.5 ($n = 21$)	5.8 ± 1.0^{a} ($n = 5$)	4.3 ± 1.0 ($n = 8$)	$17 \pm 1.0^{a,b}$ ($n = 8$)	$9.5 \pm 1.5^{a,b}$ ($n = 4$)	3.4 ± 1.5 ($n = 4$)

[a] $p < 0.05$ when compared with Kv4.2 alone, two-tailed (independent) *t* test.
[b] $p < 0.05$ when compared with Kv4.2 + KChIP3a, two-tailed (independent) *t* test.
[c] ND, not determined.

FIGURE 4. **KChIP4a, KChIP2x, and KChIP3x interact with Kv4.2 and significantly interfere with KChIP-associated promotion of Kv4.2 surface expression.** *A*, effects of KChIP isoforms on Kv4.2 surface expression as determined by comparisons of peak current measurement. Change in current expression at +50 mV was calculated as -fold change increase over that of Kv4.2 channels alone. *Asterisks* indicate statistically significant difference from the Kv4.2 + KChIP3a result, as determined by independent two-tailed Student's *t* test. The number of trials is shown in *parentheses*. *B*, coimmunoprecipitation of KChIP3a, KChIP3x, KChIP2x, and KChIP4a with Kv4.2 expressed in HEK293T cells. Goat anti-Kv4.2 antibody, but not goat IgG, pulled down Kv4.2 proteins and coprecipitated the associated KChIP proteins.

KChIP4a, KChIP2x, and KChIP3x all induce rightward, ~25–30-mV shifts in the midpoint of the *G*-V relationship when compared with KChIP3a or KChIP4b-L (Table 1). KChIP2x and KChIP3x, but not KChIP4a, also increase the steepness of the *G*-V curve, suggesting an increase in voltage sensitivity (Fig. 4*E*). The differential effects of KIS variants on voltage-dependent gating are further supported by studies of steady-state inactivation of Kv4.2 co-expressed with various KChIPs. KChIP2x and KChIP3x both produce similar ~10-mV depolarizing shifts in the voltage dependence of steady-state inactivation when compared with KChIP3a or KChIP4b-L (Fig. 4*F* and Table 1). In contrast, KChIP4a had no effect on this voltage-dependent parameter. These results suggest that modulation of Kv4.2 cur-

rents by the KISD-containing KChIP variants include a combination of positive shifts in voltage-dependent gating and alterations in kinetic rates in inactivation and recovery from inactivation.

KISDs Suppress Surface Expression of Kv4.2 Channels—Aside from changes in Kv4 gating properties, the KChIP4a KISD exerts a large effect on channel trafficking. The KISD on KChIP4a completely blocks the enhanced surface expression of Kv4.2 seen with non-KISD-containing KChIP variants (7, 13). In COS-1 cells, the immunostaining pattern of KChIP4a with or without Kv4.2 is perinuclear and possibly associated with ER (13). We therefore tested if the other KISD variants also lead to the subsurface retention of Kv4.2. Normalized against Kv4.2 expressed alone, the non-KIS variant KChIP3a enhanced the Kv4.2 surface expression by ~9.5-fold, as measured by peak current at +50 mV (Fig. 4*A*). KChIP4a, in contrast, produced no significant changes in surface expression, and KChIP3x and KChIP2x both significantly decreased the amount of current enhancement normally associated with KChIP interaction. This result is consistent with the KISDs suppressing trafficking of Kv4.2 channels to the surface.

To determine if the differences in surface expression of Kv4.2 channels co-expressed with KChIP3a, KChIP4a, KChIP2x, or KChIP3x are produced by changes in the interaction between the Kv4.2α- and KChIP modulatory subunits, co-immunoprecipitations experiments were performed. As shown in Fig. 4*B*, anti-Kv4.2 antibody immunoprecipitated KChIP3a along with Kv4.2 when the two proteins were coexpressed in HEK293T cells. When Kv4.2 was co-expressed with KChIP4a, KChIP2x, or KChIP3x, anti-Kv4.2 antibody equally effectively pulled down the respective KISD-containing KChIP variants, suggesting that decreased surface expression does not appear to be produced by a decreased molecular interaction of Kv4.2 with KChIP4a, KChIP2x, and KChIP3x (Fig. 4*B*).

Shibata *et al.* (13) showed that KChIP4a, when expressed alone in COS-1 cells, is retained in the perinuclear ER/Golgi, suggesting that the KISD variable region is functioning as an ER retention signal. To test the generality of this hypothesis, we next sought to determine if the observed ER retention property could be transferred to another protein by fusing the different KISDs to eGFP. Thus, we genetically engineered cDNAs encoding fusion proteins with N-terminal KISDs linked at the C terminus to eGFP. The expression of fusion proteins were driven by the pCMV promoter during transient expression in HEK293T cells, and the subcellular distribution of this fusion construct was then monitored by fluorescent confocal microscopy.

The distribution of eGFP expressed alone in HEK293T cells is diffuse and not limited by nuclear or cytoplasmic compartmentalization (Fig. 5, *A1*). Nonfluorescent intracellular structures can clearly be identified as nucleoli, nuclear membrane, and perinuclear ER (Fig. 5*A2*). N-terminal attachment of the KChIP4a KISD to eGFP (4aNt-eGFP) completely alters the subcellular distribution (Fig. 5*B1*). 4aNt-eGFP proteins are not diffusely distributed throughout the cell; instead, they are excluded from the nucleus and restricted to the intracellular membrane network throughout the cell, particularly the perinuclear membranes (Fig. 5*B2*). When the KISDs of

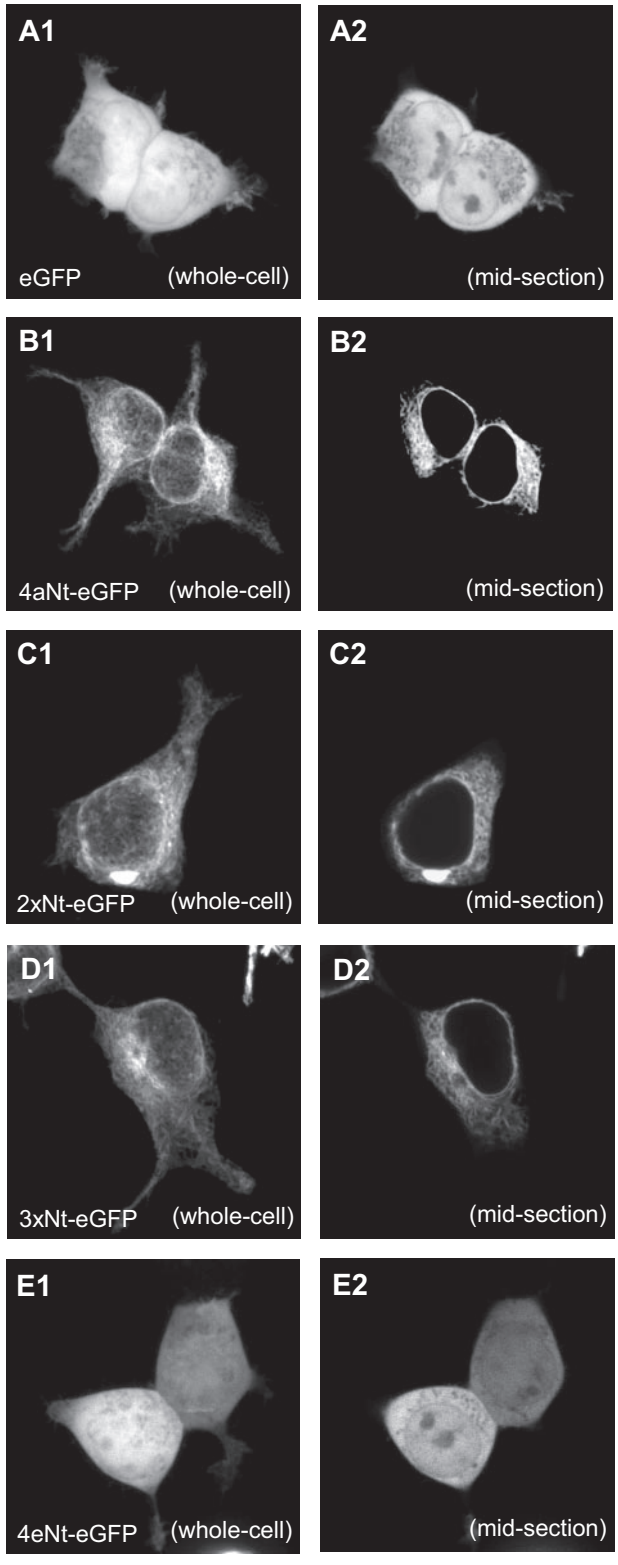

FIGURE 5. **KISDs of KChIP4a, KChIP2x, and KChIP3x all independently mediate association with ER membranes and intracellular retention.** Variable N-terminal domains of KChIP isoforms were fused with eGFP, and the wild-type eGFP and fusion proteins were expressed in HEK293T cells and imaged by confocal fluorescent microscopy. Representative cells are shown for wild-type eGFP (*A1* and *A2*), eGFP fused with KChIP4a N-terminal domain (*4aNt-eGFP*) (*B1* and *B2*), eGFP fused with KChIP2x N-terminal domain (*2xNt-eGFP*) (*C1* and *C2*), eGFP fused with KChIP3x N-terminal domain (*3xNt-eGFP*) (*D1* and *D2*), and eGFP fused with KChIP4e N-terminal domain (*4eNt-eGFP*) (*E1* and *E2*). Whole cell images generated by merging vertically stacked scans are shown in *column A1–E1*, and single images through the cell midsection are shown in *column A2–E2*.

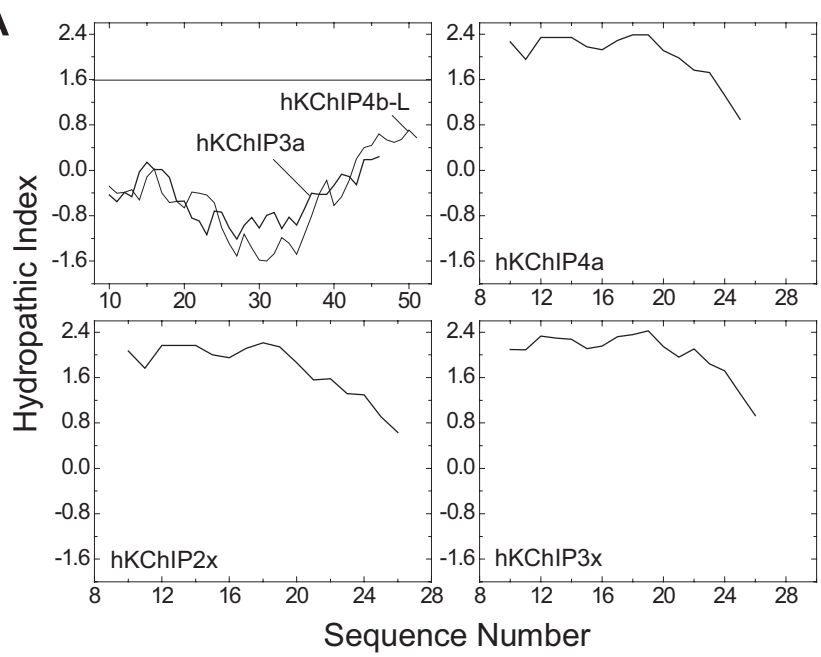

B

```
                    10        20        30
hKChIP4a        MNLEGLEMIAVLIVIVLFVKLLEQFGLIEAGLED
                ----OOOOXXXXXXXXXXIIII++++++++++      MEMSAT3
                ---TTTTTTTTTTTTTTTTT++++++++++        TMpred

                    10        20        30
hKChIP2x        MNLEGLEMVAVLVVLALFVKVLEQFGLFEPVSLED
                ----OOOOXXXXXXXXXXIIII++++++++++++    MEMSAT3
                --TTTTTTTTTTTTTTTT++++++++++++++      TMpred

                    10        20        30
hKChIP3x        MGIQGMELCAMAVVVLLFIAVLKQFGILEPISMED
                ----OOOOXXXXXXXXXXIIII++++++++++++    MEMSAT3
                --TTTTTTTTTTTTTTTTTTT++++++++++++     TMpred
```

FIGURE 6. **Hydropathy plots and statistical analyses of naturally occurring transmembrane proteins predict that KISDs of KChIP4a, KChIP2x, and KChIP3x contain a transmembrane domain.** *A*, hydropathic indices for the variable N-terminal domains of human KChIP3a, KChIP4b-L, KChIP4a, KChIP2x, and KChIP3x as a function of sequence number. The hydropathy scale is based on Kyte and Doolittle (28), and a window of 19 residues was used. A residue with a value greater than +1.6 (represented by *horizontal lines*) has a high probability of being in a transmembrane segment. *B*, implementation of MEMSAT3 and TMpred programs in predicting segment length and orientation for KChIP4a, KChIP2x, and KChIP3x. +, inside loop; −, outside loop; *O*, outside helix cap; *X*, central transmembrane helix segment; *I*, inside helix cap; *T*, transmembrane.

KChIP2x and KChIP3x are fused to eGFP (2xNt-eGFP and 3xNt-eGFP), they also similarly mediate perinuclear membrane localization of eGFP molecules (Fig. 5, *C1* and *C2*; *D1* and *D2*).

To demonstrate that the ER retention of the fusion proteins was contingent on the KISD sequence, we also fused the variable N-terminal domain of KChIP4e to eGFP (4eNt-eGFP). Although the N-terminal domain of KChIP4e has more hydrophobic content than most KChIP N terminus (hydrophobic residues underlined: MLTLEWESEGLQTVGIVVIICASLKLLHLLGLIDFSED), as Fig. 5, *E1* and *E2*, shows, 4eNt-eGFP fluorescence is distributed diffusely throughout HEK293T cells, indistinguishable from wild-type eGFP signals. We therefore reasonably conclude that the KISD targets proteins to intracellular membranes, thus interfering with surface trafficking of bound Kv4.2 channels.

Hydropathy Analysis of the KISDs of KChIP4a, KChIP2x, and KChIP3x—We next sought to understand the function of the KIS element, the conserved core motif present in the KISD. The most pronounced characteristic of the KIS element is its hydrophobic nature, with a long stretch of uninterrupted hydrophobic residues in KChIP4a (12 residues), KChIP2x (12 residues), and KChIP3x (15 residues) (Fig. 1*A*). These hydrophobic stretches are flanked N-terminally by an acidic residue (*E*) and C-terminally by a basic residue (*K*) and are suggestive of a transmembrane domain. In addition, the canonical residues of the KIS element are spaced every 3–4 residues, suggestive of a conserved interaction interface on a transmembrane α-helix (Fig. 1*A*).

To further investigate this possibility, we first simply analyzed the hydropathic profile of the variable N-terminal domains of non-KISD- and KISD-containing KChIP isoforms using the Kyte-Doolittle algorithm with a "sliding window" approach (28). In this approach, if the mean hydropathic value calculated for any 19-residue window is greater than +1.6, then there is a high probability that the center residue resides within a membrane-spanning helix. The hydropathy plots reveal that the N-terminal domains of KChIP3a and KChIP4b-L, as expected, are quite polar and inconsistent with transmembrane domains (Fig. 6*A*). In contrast, the hydrophobic segments of KChIP4a, KChIP2x, and KChIP3x KISDs are consistent with being transmembrane domains, all containing 19 residue windows with hydrophobic indices greater than 2.0 (Fig. 6*A*). To refine our analyses of the potential transmembrane KISDs, the MEMSAT3 program was used (18, 19). MEMSAT3 reportedly does an excellent job of predicting single pass transmembrane segments with a high success rate of 98%. Results of the MEMSAT3 prediction suggest that a ≥19-amino acid long transmembrane domain is present in the KISDs of KChIP4a, KChIP2x, and KChIP3x (Fig. 6*B*). This predicted transmembrane domain encompasses the entire KIS element previously identified from homology analysis.

Finally, we also analyzed the KISDs using the TMpred program to predict the membrane-spanning regions and their orientation (20). The TMpred (transmembrane prediction) algo-

rithm uses weight matrices extracted from statistical analyses of naturally occurring transmembrane proteins present in the SwissProt data base. The TMpred program also predicts a transmembrane domain within the KISD with slight differences in the beginning and end of this TM domain between different isoforms (Fig. 6*B*). For KChIP4a, the predicted transmembrane domain begins at Glu^4 and ends at Leu^{23}, for a length of 20 amino acids, which is similar to the 19 residues predicted by MEMSAT3. For KChIP2x, the predicted transmembrane domain begins at Leu^3 and ends at Val^{19}, giving a length of 17 residues, which is 2 residues shorter than predicted by MEMSAT3. TMpred predicted the transmembrane domain in KChIP3x KISD to begin at Ile^3 and end at Leu^{22}, similar to the MEMSAT3 prediction for KChIP3x. In conclusion, Kyte-Doolittle, MEMSAT3, and TMpred analyses all predict that the KIS element within the KISDs probably forms a transmembrane domain, which in KChIP4a runs from approximately residues 3–5 and ends at residues 19–23.

Subcellular Localization of KIS Variant KChIPs in Mammalian Cells—If KISDs contain a transmembrane domain, then we would predict that KChIPs containing these domains should be localized to membrane compartments. To test this hypothesis, HEK293T cells expressing various KChIPs were collected and mechanically lysed, and crude membranes were separated from intact nuclei, organelles, cells, and cell debris. The membranes were recovered by centrifugation, and the membrane proteins were solubilized and separated on SDS-PAGE for analysis. As controls for the procedure, we also processed cells expressing known transmembrane (DPP6-S and DPP6a) and cytosolic (eGFP) proteins. Dipeptidyl peptidase 6-S (short) and 6a proteins (DPP6-S and DPP6a), also respectively known as DPPX-S and DPPX-E, are type II transmembrane proteins of ~115 kDa (6), and the membrane preparation procedure clearly separated these transmembrane proteins into the membrane fraction without any observable leaching into the cytosolic fraction (Fig. 7*A*). Meanwhile, cytosolic eGFP is recovered exclusively in the cytosolic fraction (Fig. 7*C*).

As controls for KChIPs lacking KISDs, we next performed tests with KChIP3a and KChIP4b N-terminal variants (Fig. 7*B*). KChIP3a proteins are reported to be distributed throughout the cytoplasm of transfected cultured cells (29), but a small fraction may be associated with membrane due to palmitoylation of cysteine residues in the variable domain (30). In agreement with published results, our results show that the majority of KChIP3a proteins are cytosolic; however, a small but significant fraction is also isolated along with the membrane fraction, probably as a result of KChIP3a palmitoylation (Fig. 7*B*). The variable N-terminal domain of KChIP4b contains no site for palmitoylation or myristoylation, lipid modifications that affect KChIP3 and KChIP1, respectively (30, 31). Fractionation of KChIP4b expressed in HEK293T cells show that it is exclusively localized in the cytosolic fraction (Fig. 7*B*).

We next tested KISD-containing KChIPs. The results show that KChIP4a proteins, like DPP6-S and DPP6a proteins, are mostly present in the membrane fraction and not in the cytosolic fraction (Fig. 7*B*). Likewise, KChIP2x and KChIP3x proteins are found mostly in the membrane fraction, with a small amount detected in the cytosolic fraction. To biochemically test if the observed subcellular distribution of KISD-tagged GFP proteins is due to KISD targeting of GFP to membranes, we performed subcellular fraction of HEK293T cells expressing 4aNteGFP, 2xNt-eGFP, 3xNt-eGFP, and 4eNt-eGFP. As predicted from the fluorescence patterns, we find that 4aNt-, 2xNt-, and 3xNt-eGFPs are isolated in the membrane fraction, whereas 4eNt-eGFP is found only in the cytosolic fraction (Fig. 7*C*). These results suggest that KChIP4a, KChIP2x, and KChIP3x are associated with the membrane as a result of a predicted KISD transmembrane domain.

Surface Biotinylation Results Show That the KIS Element Forms a Transmembrane Domain—Our results thus far support a transmembrane topology for the KISDs of KChIP4a, KChIP2x, and KChIP3x; however, the results we have obtained thus far could be due to interactions of the KISD with other membrane-localized elements rather than the KIS element being itself a transmembrane domain. To provide more direct evidence that the KIS element is transmembrane, we sought to test if cysteine residues introduced into the N terminus of the protein could be labeled by biotinylation reagents applied to the outside of cells. Because most of the KISD-containing KChIP proteins are retained in intracellular membranes, we expected that this labeling might be inefficient; however, we do know from physiological experiments that a fraction of the protein is present on the cell surface. For these studies, we used the well characterized KChIP4a protein and mutated either position 2 or 4 to cysteine. Asn^2 and Glu^4 were good candidates for cysteine mutations, because positions 2 and 4 are not conserved between KChIP4a, KChIP2x, and KChIP3x (Fig. 1*A*). We performed surface biotinylation by reacting surface cysteines with a membrane-impermeant biotin-conjugated maleimide (maleimide-PEO2-biotin). To check that the cells are not damaged during the biotinylation procedure, thus potentially leading to false surface biotinylation signals, HEK293T cells expressing eGFP were processed the same way as KChIP4a-expressing cells. As shown in Fig. 8*B*, cytoplasmic eGFP is not biotinylated by extracellular application of maleimide-PEO2-biotin. Likewise, prior to introduction of cysteine residues, no surface biotinylation occurs with wild-type KChIP4a expressed in HEK293T cells (Fig. 8*A*). If the cells are lightly permeabilized by Triton X-100, then wild-type KChIP4a can be biotinylated on intracellularly located cysteine residues, indicating that the biotinylation reaction is working as expected. Reduced signal upon permeation by Triton X-100 results from the tendency of cells to detach under such conditions.

In contrast to our previous results with cytoplasmically localized proteins, substitution of cysteine for asparagine at position 2 of KChIP4a allows the protein to react with extracellularly applied maleimide-PEO2-biotin (Fig. 8*A*). Results show that, as expected, a somewhat weak signal was detected, since only a minute fraction of KChIP4a in the total lysate came from the cell surface, due to ER retention. Exposing the entire population of proteins to reagent by permeabilization of the cells leads to significantly more KChIP4a/N2C recovered by biotinylation pull-down. Interestingly, when glutamate at position 4 was mutated to cysteine, making KChIP4a/E4C, this introduced cysteine residue could not be modified by maleimide-PEO2-biotin. Because cysteine is a

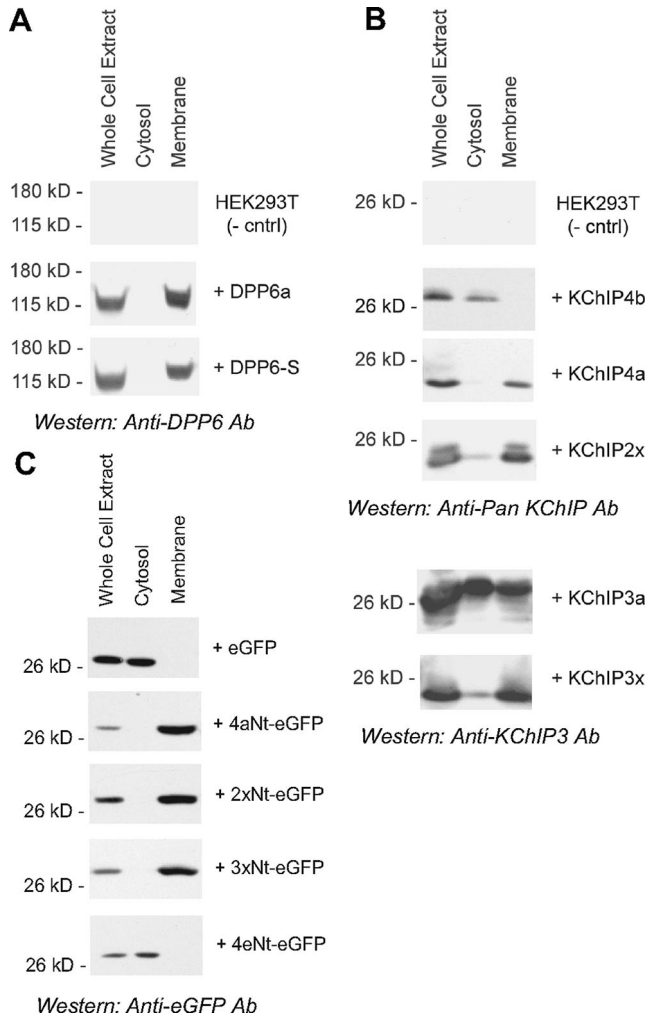

FIGURE 7. **KChIP4a, KChIP2x, and KChIP3x tend to segregate in lipid membranes.** *A*, Western analyses of crude membrane preparations from HEK293T-expressed control proteins, including both type II transmembrane proteins (DPP6a and DPP6-S) and cytosolic proteins (eGFP). DPP6a and DPP6-S show membrane segregation, with no observable contamination of cytosolic fraction. eGFP is detected only in the cytosolic fraction, as expected. *B*, differential subcellular compartmentalization of KISD-containing and non-KISD-containing KChIP variants. KChIP4b exhibits strict localization in the cytosol, and although KChIP3a also prefers an aqueous, cytosolic environment, a significant proportion is associated with membrane. KChIP4a, KChIP2x, and KChIP3x proteins show strong association with membrane lipids. *C*, transfer of KISDs to eGFP produces membrane association of the protein. N-terminal fusion with KChIP4a, KChIP2x, and KChIP3x KISDs results in eGFP association with membrane fraction. The N-terminal variable domain of KChIP4e has no effect on eGFP subcellular fractionation.

hydrophobic residue, it is likely that this side chain is localized in the membrane and thus inaccessible to maleimide-PEO2-biotin. When both Asn^2 and Glu^4 are mutated to cysteine (KChIP4a/N2C/E4C), the protein is biotinylated about as well as KChIP4a/N2C. These results strongly support the hypothesis that the KIS element encodes a Type I transmembrane domain with very few extracellularly exposed residues.

DISCUSSION

We have discovered that KChIP4a, a KChIP4 N-terminal variant recognized for its unusual ability to eliminate Kv4 fast inactivation, belongs to a special group of KChIP isoforms with similar functional properties. The members of this group, including KChIP4a, KChIP2x, and KChIP3x, possess an N-terminal membrane-spanning segment that would classify them as type I integral membrane proteins. The presence of this transmembrane domain at the N terminus of KChIPs is associated with severe disruption of Kv4 inactivation and ER retention of Kv4 proteins. However, its presence does not strictly determine how channel properties are modified, resulting in a diversity of kinetic and voltage-dependent gating properties.

Multiple KChIP Isoforms Have KISDs—The major focus for molecular studies on neuronal I_{SA} has been on identifying auxiliary subunits that produce fast rapid activation and inactivation gating (25, 32, 33), making KChIP4a a curiosity among the I_{SA} subunits. Here we show that KChIP4a is no lone oddball but rather is one member of a group of KChIPs that modify I_{SA} channel expression and functional properties by providing an additional regulatory transmembrane domain that modifies the functional properties of the transmembrane pore gates. KISD-containing isoforms, KChIP2x, KChIP3x, and KChIP4a, are therefore probably responsible for important distinctive kinetic changes in native A-currents where they are expressed. Recently, studies on the expression of KChIP transcripts have shown that both KChIP4a and KChIP3x/3b exhibit diffuse expression pattern in the central nervous system (5). Indeed, the apparent broad distribution of KISD-containing KChIPs expression in the brain would suggest that such slow Kv4-based A-currents are more widely distributed than previously thought. Two important factors, however, may limit the extent of inactivation slowing produced by these KIS-ing cousins: 1) KISD-containing channel express less well on the cell surface, leading to functional underrepresentation; 2) certain DPLP isoforms, such as DPP10a, may dominantly determine the inactivation kinetics at depolarized potentials even if KISD subunits are present (8). Although DPP10a overrides KChIP4a at depolarized potential by mediating ultrafast inactivation, at more modest potentials, where neurons typically operate, measurable effects of KChIP4a can still be seen. For example, the influence of KChIP4a on Kv4.2 + DPP10a channels is detectable as an ~15-mV depolarizing shift in the *G*-V relationship and slower recovery from inactivation (8). Although beyond the scope of the present work, it would highly informative to determine the combinatorial effects produced when KChIP2x and KChIP3x are co-expressed in the presence of different DPLPs.

The KISD Contains a Transmembrane Segment—The discovery that the KISD contains a transmembrane segment suggests that KChIP4a, KChIP2x, and KChIP3x comprises a novel class of KChIP isoforms, type I integral membrane KChIP proteins with a C-terminal Kv4-interacting core (Fig. 9*A*). To better understand how the KISD might function, it would be instructive to consider MiRP1, the gene product of KCNE2. MiRP1 is another type I transmembrane protein that reportedly forms stable associations with Kv4.2 and Kv4.3 channels and modifies gating kinetics (34, 35). Interestingly, several distinctive effects of MiRP1 on Kv4.2 are similar to those of KChIP4a, KChIP2x, and KChIP3x: marked slowing of activation kinetics, slowing of inactivation kinetics, and a lack of dramatic increase in surface expression (34). An unusual effect shared by MiRP1, KChIP4a, and KChIP2x is an overshoot of Kv4.2 peak current

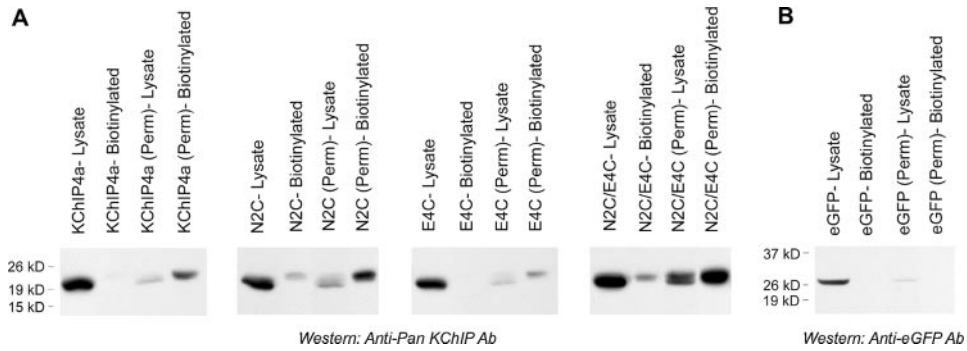

FIGURE 8. **Surface biotinylation results show that KChIP4a KISD is transmembrane where N2, but not E4, is exposed on the HEK293T cell surface.** *A*, streptavidin pull-down of surface biotinylated KChIP4a wild-type and N-terminal cysteine mutants (N2C, E4C, and N2C/E4C). As control, transfected HEK293T cells were also permeabilized (*Perm*) to check for reagent reactivity. Surface biotinylation occurs for KChIP4a/N2C and KChIP4a/N2C/E4C, but E4 is nonreactive. *B*, experimental control for membrane integrity of HEK293T cells. Cytosolic eGFP in intact cells was unavailable for reaction with biotinylation reagent, and the permeabilization process releases eGFP and results in loss of eGFP signal.

amplitude during recovery from inactivation (Fig. 3*C* and Table 1). These results suggest that the transmembrane segments of KChIP4a, KChIP2x, and KChIP3x, like the MiRP1 transmembrane segment, mediate similar functional effects on channel gating. In agreement, a molecular dynamic simulation of KChIP2x-bound Kv4.2 channel in a lipid bilayer environment shows that the KIS element is stable in the bilayer close in proximity to the channel pore-forming and voltage-sensing domains (Fig. 9*B*).

The transmembrane nature of the KISD also suggests a hypothetical molecular basis that explains the marked depolarizing shifts in the voltage dependence of activation and inactivation mediated by KChIP2x and KChIP3x (Fig. 3, *E* and *F*, and Table 1). The transmembrane DPP6 auxiliary subunit alters channel gating by impacting voltage sensor movement (36); perhaps transmembrane KISD changes voltage dependence of gating by slowing down voltage sensor movement, leading to the concomitant rightward shifts in voltage dependence.

The KISD Transmembrane Segment Mediate ER Retention—Expression of fusion proteins between eGFP and KISDs targets eGFP to intracellular membranes, directly demonstrating that KISDs mediate intracellular retention. Interestingly, the integral association of these KChIPs to the membrane by a transmembrane segment produces results opposite from those of fatty acid modification used by other KChIPs. Myristoylation of KChIP1 is necessary and sufficient to target KChIP1 to the post-ER pre-Golgi transport vessicles, thereby promoting efficient trafficking of Kv4.2 channels to the cell surface (31). Similarly, palmitoylation of KChIP3a, KChIP2a, and KChIP2b is required for effective cell surface localization and enhancement of Kv4.2 current expression (30). Similar to KISD-containing KChIPs, the transmembrane MiRP2 subunits are also retained in the ER; however, they are released following coassembly with KCNQ subunits (37).

Precisely how the KISD mediates ER retention is unknown and beyond the scope of this work. However, it is thought that ER retention of type I membrane proteins occurs through both retention signal-dependent and signal-independent mechanisms. Many ER-resident proteins in animal cells contain a cytosolic dilysine motif (KK*XX* or K*X*K*XX*) at the C-terminal end (38–42). This retention signal-based mechanism seems unlikely, considering that the C-terminal end is shared between different KChIP isoforms. Instead, the KISD probably utilizes a signal-independent mechanism of ER retention (43).

Alternative Hypothesis—During the preparation of this manuscript, Schwenk *et al.* (44) described an NMR analysis of an N-terminal His_6-tagged KChIP4a molecule under cell-free, lipid-free conditions. Their data indicate that the KISD consists of a six-turn α-helix and a solvent-exposed linker. The location of the α-helix, between Glu^4 and Gln^{24} of KChIP4a, closely matches our prediction of transmembrane segment between residues 3–5 and 20–23.

In addition, Schwenk et al. (44) found that *in vitro* the KISD hydrophobic domain could bind to the KChIP core in an autoinhibitory manner. Our work suggests that when expressed in a normal cellular environment, the KISD mediates association with intracellular membranes and forms a transmembrane domain that would not be expected to have access to the cytoplasmic KChIP core. Furthermore, our coimmunoprecipitation results show that the presence of KISD on KChIP4a, KChIP2x, and KChIP3x does not significantly decrease the association with Kv4.2 channels in comparison with non-KISD-containing KChIP3a (Fig. 4*B*), contradicting the idea that in the native environment, KISD effectively competes with the Kv4.2 N-terminal domain for the KChIP hydrophobic pocket. Finally, if the KChIP4a KISD effectively autoinhibits the binding with the Kv4.2 N terminus, the N-type inactivation kinetics should be revealed, producing rapid inactivation that accelerates with depolarization (14). Instead, an inverse relationship between inactivation and voltage is observed with KChIP4a, KChIP2x, and KChIP3x (Fig. 3*B*). We would suggest that, in a cellular environment, it is more likely that the KISD inserts itself into the lipid bilayer than interacting with its own hydrophobic pocket. As a whole, our model of the KISD mechanism of action effectively offers a reasonable explanation for the effects on both surface expression and gating modulation.

Physiological Consequences and Relevance—With our discovery of a family of type I transmembrane KChIP isoforms, we have introduced another layer of complexity to the formation of the I_{SA} channel complex. Auxiliary subunits of Kv4 channels now reportedly come in four types: cytoplasmic with fatty acid modifications (myristoylation of KChIP1, palmitoylation of KChIP2 and KChIP3a), type II transmembrane (DPLP isoforms: DPP6 and DPP10), type I transmembrane (MiRPs), and type I transmembrane KChIPs (tmKChIPs; KChIP4a, KChIP2x, and KChIP3x) (Fig. 9*A*). Possessing structural elements of both MiRPs and KChIPs, tmKChIPs may compete with MiRP1 and KChIPs for interaction sites and influence the selection of subunit composition of native I_{SA} channels. Tinel *et al.* (45) reported that MiRP1 exhibits a neuronal expression in, among

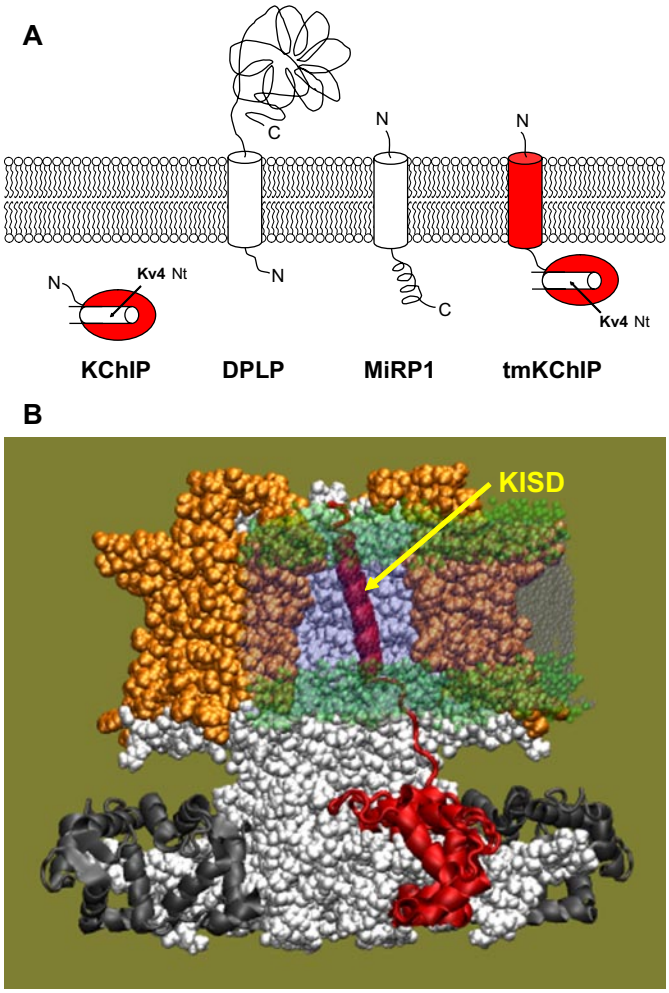

FIGURE 9. **tmKChIPs, a novel class of Kv4 modulatory subunit.** *A*, schematic diagram describing the known types of Kv4 modulatory subunits. All KChIP subunits possess a binding pocket for the hydrophobic cytoplasmic N terminus of Kv4 channels (*Kv4 Nt*). Isoforms without an N-terminal transmembrane domain typically display a cytosolic distribution, unless post-translationally modified by fatty acid linkage (myristoylation and palmitoylation) (modification not shown). DPLPs (DPP10 and DPP6) are type II transmembrane proteins with the N terminus inside and C terminus outside. MiRP1 modulate Kv4 channels and represent a type I transmembrane protein with an extracellular N terminus. tmKChIPs (KChIP4a, KChIP2x, and KChIP3x) are also type I transmembrane proteins, with KChIP core domains that interact with the Kv4 N terminus. *B*, molecular dynamic modeling of KChIP2x subunit bound to Kv4.2 α-subunits surrounded in a lipid bilayer. Molecular simulation also includes salt conditions for the intracellular and extracellular milieu. The 6-turn α-helix of the KChIP2x KISD (*red*), attached to the KChIP2 core domain via a linker, is predicted to insert into the lipid bilayer (in *green*) between the Kv4.2 voltage sensors (*yellow*). Other Kv4 N termini are bound by KChIP core domains only (*black*). The Kv4.2 channel, other than the voltage sensors, is shown in *white*.

other locations, cerebellum, neocortex, piriform cortex, hippocampal formation, thalamus, and hypothalamus. This pattern of expression overlaps those of KChIP4a and KChIP3x (5). Further work will be required to determine the native partners of Kv4-based A-type channels.

A common feature of KChIP4a, KChIP2x, and KChIP3x is their propensity to be retained in the ER networks, and as Shibata *et al.* (13) showed, KChIP4a is a potent and specific suppressor of increased Kv4.2 surface expression induced by other KChIP isoforms. However, when Kv4.2 is coexpressed with both KChIP4a and DPP6-S, the current amplitude is dramatically increased (data not shown), whereas the inactivation kinetics resembles that of Kv4.2 + KChIP4a channels (8). This suggests that DPP6-S and perhaps other DPLPs interacts with Kv4.2 and may be necessary for efficient surface expression of I_{SA} in neurons that express tmKChIPs. This may occur by the integration of DPLPs into the Kv4.2-KChIP4a binary complex, directly promoting the surface expression by overcoming the tmKChIP tendency to be retained in the ER, as discussed above. Indeed, the retention function of tmKChIPs may play a major role in deciding whether a channel complex is ready to be trafficked to the surface as a complete multisubunit complex, a function critical for I_{SA} quality control and neuronal physiology.

Acknowledgments—We thank Dr. Lily Jan for providing the Kv4.2 cDNA. We also think Alison Prince Carter for assisting in harvesting oocytes for the functional studies.

REFERENCES

1. Jerng, H. H., Pfaffinger, P. J., and Covarrubias, M. (2004) *Mol. Cell Neurosci.* **27,** 343–369
2. An, W. F., Bowlby, M. R., Betty, M., Cao, J., Ling, H. P., Mendoza, G., Hinson, J. W., Mattsson, K. I., Strassle, B. W., Trimmer, J. S., and Rhodes, K. J. (2000) *Nature* **403,** 553–556
3. Nadal, M. S., Ozaita, A., Amarillo, Y., Vega-Saenz de Miera, E., Ma, Y., Mo, W., Goldberg, E. M., Misumi, Y., Ikehara, Y., Neubert, T. A., and Rudy, B. (2003) *Neuron* **37,** 449–461
4. Jerng, H. H., Qian, Y., and Pfaffinger, P. J. (2004) *Biophys. J.* **87,** 2380–2396
5. Pruunsild, P., and Timmusk, T. (2005) *Genomics* **86,** 581–593
6. Nadal, M. S., Amarillo, Y., Vega-Saenz de Miera, E., and Rudy, B. (2006) *Brain Res.* **1094,** 1–12
7. Holmqvist, M. H., Cao, J., Hernandez-Pineda, R., Jacobson, M. D., Carroll, K. I., Sung, M. A., Betty, M., Ge, P., Gilbride, K. J., Brown, M. E., Jurman, M. E., Lawson, D., Silos-Santiago, I., Xie, Y., Covarrubias, M., Rhodes, K. J., Distefano, P. S., and An, W. F. (2002) *Proc. Natl. Acad. Sci. U. S. A.* **99,** 1035–1040
8. Jerng, H. H., Lauver, A. D., and Pfaffinger, P. J. (2007) *Mol. Cell Neurosci.* **35,** 604–624
9. Zhou, W., Qian, Y., Kunjilwar, K., Pfaffinger, P. J., and Choe, S. (2004) *Neuron* **41,** 573–586
10. Scannevin, R. H., Wang, K., Jow, F., Megules, J., Kopsco, D. C., Edris, W., Carroll, K. C., Lu, Q., Xu, W., Xu, Z., Katz, A. H., Olland, S., Lin, L., Taylor, M., Stahl, M., Malakian, K., Somers, W., Mosyak, L., Bowlby, M. R., Chanda, P., and Rhodes, K. J. (2004) *Neuron* **41,** 587–598
11. Wang, H., Yan, Y., Liu, Q., Huang, Y., Shen, Y., Chen, L., Chen, Y., Yang, Q., Hao, Q., Wang, K., and Chai, J. (2007) *Nat. Neurosci.* **10,** 32–39
12. Pioletti, M., Findeisen, F., Hura, G. L., and Minor, D. L., Jr. (2006) *Nat. Struct. Mol. Biol.* **13,** 987–995
13. Shibata, R., Misonou, H., Campomanes, C. R., Anderson, A. E., Schrader, L. A., Doliveira, L. C., Carroll, K. I., Sweatt, J. D., Rhodes, K. J., and Trimmer, J. S. (2003) *J. Biol. Chem.* **278,** 36445–36454
14. Gebauer, M., Isbrandt, D., Sauter, K., Callsen, B., Nolting, A., Pongs, O., and Bahring, R. (2004) *Biophys. J.* **86,** 210–223
15. Beck, E. J., Bowlby, M., An, W. F., Rhodes, K. J., and Covarrubias, M. (2002) *J. Physiol.* **538,** 691–706
16. Baranauskas, G. (2004) *Eur. J. Neurosci.* **20,** 385–391
17. Jerng, H., and Pfaffinger, P. J. (2008) *Biophys. J.* **94,** 521
18. Jones, D. T. (2007) *Bioinformatics* **23,** 538–544
19. Jones, D. T., Taylor, W. R., and Thornton, J. M. (1994) *Biochemistry* **33,** 3038–3049
20. Hofmann, K., and Stoffel, W. (1993) *Biol. Chem. Hoppe-Seyler* **374,** 166
21. Long, S. B., Tao, X., Campbell, E. B., and MacKinnon, R. (2007) *Nature* **450,** 376–382
22. Guex, N., and Peitsch, M. C. (1997) *Electrophoresis* **18,** 2714–2723
23. Humphrey, W., Dalke, A., and Schulten, K. (1996) *J. Mol. Graph.* **14,**

27–38
24. Schultz, J. H., Volk, T., Bassalay, P., Hennings, J. C., Hubner, C. A., and Ehmke, H. (2007) *Pfluegers Arch. Eur. J. Physiol.* **454,** 195–207
25. Jerng, H. H., Kunjilwar, K., and Pfaffinger, P. J. (2005) *J. Physiol.* (*Lond*.) **568,** 767–788
26. Jerng, H. H., Shahidullah, M., and Covarrubias, M. (1999) *J. Gen. Physiol.* **113,** 641–660
27. Amarillo, Y., De Santiago-Castillo, J. A., Dougherty, K., Maffie, J., Kwon, E., Covarrubias, M., and Rudy, B. (2008) *J. Physiol.* (*Lond*.) **586,** 2093–2106
28. Kyte, J., and Doolittle, R. F. (1982) *J. Mol. Biol.* **157,** 105–132
29. Woo, H. N., Chang, J. W., Choi, Y. H., Gwon, A. R., Jung, Y. K., and Jo, D. G. (2008) *Neuroreport* **19,** 1193–1197
30. Takimoto, K., Yang, E. K., and Conforti, L. (2002) *J. Biol. Chem.* **277,** 26904–26911
31. O'Callaghan, D. W., Hasdemir, B., Leighton, M., and Burgoyne, R. D. (2003) *J. Cell Sci.* **116,** 4833–4845
32. Rudy, B., Hoger, J. H., Lester, H. A., and Davidson, N. (1988) *Neuron* **1,** 649–658
33. Chabala, L. D., Bakry, N., and Covarrubias, M. (1993) *J. Gen. Physiol.* **102,** 713–728
34. Zhang, M., Jiang, M., and Tseng, G. N. (2001) *Circ. Res.* **88,** 1012–1019
35. Deschenes, I., and Tomaselli, G. F. (2002) *FEBS Lett.* **528,** 183–188
36. Dougherty, K., and Covarrubias, M. (2006) *J. Gen. Physiol.* **128,** 745–753
37. Chandrasekhar, K. D., Bas, T., and Kobertz, W. R. (2006) *J. Biol. Chem.* **281,** 40015–40023
38. Jackson, M. R., Nilsson, T., and Peterson, P. A. (1990) *EMBO J.* **9,** 3153–3162
39. Townsley, F. M., and Pelham, H. R. (1994) *Eur. J. Cell Biol.* **64,** 211–216
40. Letourneur, F., Gaynor, E. C., Hennecke, S., Demolliere, C., Duden, R., Emr, S. D., Riezman, H., and Cosson, P. (1994) *Cell* **79,** 1199–1207
41. Nilsson, T., Jackson, M., and Peterson, P. A. (1989) *Cell* **58,** 707–718
42. Gaynor, E. C., te Heesen, S., Graham, T. R., Aebi, M., and Emr, S. D. (1994) *J. Cell Biol.* **127,** 653–665
43. Nilsson, T., and Warren, G. (1994) *Curr. Opin. Cell Biol.* **6,** 517–521
44. Schwenk, J., Zolles, G., Kandias, N. G., Neubauer, I., Kalbacher, H., Covarrubias, M., Fakler, B., and Bentrop, D. (2008) *J. Biol. Chem.* **283,** 18937–18946
45. Tinel, N., Diochot, S., Lauritzen, I., Barhanin, J., Lazdunski, M., and Borsotto, M. (2000) *FEBS Lett.* **480,** 137–141